Nanoscale

ROYAL SOCIETY OF CHEMISTRY

PAPER

View Article Online
View Journal | View Issue

Cite this: *Nanoscale*, 2023, **15**, 1763

Structural investigations into colour-tuneable fluorescent InZnP-based quantum dots from zinc carboxylate and aminophosphine precursors†

Mary Burkitt-Gray,[a,b] Marianna Casavola,[a] Pip C. J. Clark,[c] Simon M. Fairclough,[a] Wendy R. Flavell,[c] Roland A. Fleck,[b] Sarah J. Haigh,[d] Jack Chun-Ren Ke,[c] Marina Leontiadou,[c] Edward A. Lewis,[d] Jacek Osiecki,[e] Basma Qazi-Chaudhry,[a] Gema Vizcay-Barrena,[b] Wijittra Wichiansee[a] and Mark Green *[a]

Received 20th May 2022,
Accepted 25th November 2022

DOI: 10.1039/d2nr02803d

rsc.li/nanoscale

Fluorescent InP-based quantum dots have emerged as valuable nanomaterials for display technologies, biological imaging, and optoelectronic applications. The inclusion of zinc can enhance both their emissive and structural properties and reduce interfacial defects with ZnS or CdS shells. However, the sub-particle distribution of zinc and the role this element plays often remains unclear, and it has previously proved challenging to synthesise Zn-alloyed InP-based nanoparticles using aminophosphine precursors. In this report, we describe the synthesis of alloyed InZnP using zinc carboxylates, achieving colour-tuneable fluorescence from the unshelled core materials, followed by a one-pot ZnS or CdS deposition using diethyldithiocarbamate precursors. Structural analysis revealed that the "core/shell" particles synthesised here were more accurately described as homogeneous extended alloys with the constituent shell elements diffusing through the entire core, including full-depth inclusion of zinc.

Fluorescent indium phosphide-based quantum dots (QDs) have shown promise in the fields of biological imaging,[1–3] lasing,[4,5] and light emitting diodes.[6–8] With a direct band-gap of 1.3 eV, InP fluorescence is conveniently in the visible spectral regions,[7,9,10] and core/shell QDs with photoluminescence (PL) from blue to near-infrared have been reported.[5,11] While the covalent nature of InP results in greater photostability[12] and less ionic leaching than Cd-based materials,[1,2,13] it also presents challenges to synthesising crystalline QDs with bright fluorescence.

Tris(trimethylsilyl)phosphine ($PTMS_3$) is the most commonly-used phosphorus precursor and has resulted in brightly-emitting materials.[2,7,9,10,14–16] However, it is expensive, pyrophoric, and prohibitively reactive.[11,17] Tris(dimethylamino)phosphine ($P(NMe_2)_3$) is a safer alternative and has recently produced promising InP-based QDs.[8,11,18–21] For example, Tessier *et al.* used $P(NMe_2)_3$ to synthesise fluorescent InP/ZnS QDs with the emission colour based on the identity of a halide dopant and emission linewidths as narrow as 46 nm.[11] Likewise, Yang *et al.* have recently synthesised InP/ZnS QDs from $P(NMe_2)_3$ with fluorescence quantum yields (QYs) of up to 63%,[8] while Jo *et al.* have synthesised graded InP/ZnSeS/ZnS from an aminophosphine precursor with QYs up to 87% and linewidths as narrow as 37 nm.[22]

Combining InP with Zn is a common approach to produce QDs with improved crystallinity,[10,23] fewer surface trap states,[18,20] and greater QYs than pure InP. As a smaller, harder ion, Zn also reduces the lattice dimensions of InP to provide a closer lattice match with a ZnS shell. However, the addition of zinc halides to the synthesis with $P(NMe_2)_3$ does not appear to result in the formation of Zn-alloyed materials.[18,21] For example, InP-based QDs synthesised by Buffard *et al.* contained only 3% Zn by atomic composition, regardless of the quantity of zinc halide added; Zn also did not contribute to the reaction intermediates or affect the rate of reaction.[18] Halide counter-ions, however, controlled the QD size dispersion, facilitated the reduction of P(III) to P(−III),[18,21] and improved the excitonic absorption feature of the resultant QDs.[20] Furthermore, the unshelled products of this reaction

---

[a] *Department of Physics, King's College London, The Strand, London, WC2R 2LS, UK. E-mail: mark.a.green@kcl.ac.uk*
[b] *Centre for Ultrastructural Imaging, King's College London, New Hunt's House, London, SE1 1UL, UK*
[c] *The Photon Science Institute, School of Physics and Astronomy, University of Manchester, Schuster Building, Oxford Road, Manchester, M13 9PL, UK*
[d] *Department of Materials, University of Manchester, Oxford Road, Manchester, M13 9PL, UK*
[e] *MAX IV Laboratory, Lund University, Box 118, 221 00 Lund, Sweden*

† Electronic supplementary information (ESI) available: Experimental and analysis details, including EDX spectra and maps, STEM microscopy images, SR-XPS, monochromatic XPS spectra, Raman spectroscopy, and XRD. See DOI: https://doi.org/10.1039/d2nr02803d

had a PL QY of less than 1% and a high prevalence of both electron and hole trap states.[24]

Zinc carboxylates have been widely used in the synthesis of InZnP with PTMS$_3$:[25] they are variously reported as reagents,[26–28] initiators,[29] or passivators.[29,30] Xu *et al.* have suggested that zinc carboxylates could not behave as precursors to the formation of alloyed InZnP as they are not strong oxidisers or reducing agents, have low reactivity with phosphorus, and are stable at the reaction temperatures used in a typical InP synthesis.[29,30] Zinc carboxylates were instead hypothesised to behave as surface passivators.[29,30] In contrast, Ryu *et al.* theorised that zinc acetate etched InP to result in an alloyed Zn-rich surface and a blue-shift in optical properties.[27] Notably, fluorescence has been observed from InP-based QDs synthesised with zinc carboxylates,[27,29,30] while the reaction with zinc halides typically results in non-emitting materials or those with a QY below 1%.[18,21,24] A recent study has, however, highlighted that the addition of ZnCl$_2$ to preformed myristate-capped InP QDs resulted in ligand exchange and an increase in emission quantum yield (to *ca.* 0.8%), highlighting that this system is far from fully understood.[31]

However, in the majority of studies to date, PTMS$_3$ was used as the phosphorus precursor, and zinc carboxylates were rarely explored as precursors to the formation of alloyed InZnP in the reaction with P(NMe$_2$)$_3$.

The synthesis of InZnP using P(NMe$_2$)$_3$ and zinc stearate was investigated here with the aim to produce alloyed InZnP, unlike the analogous reaction with zinc halides in which zinc does not alloy into the InP structure. A ZnS and CdS surface deposition procedure was then performed on the reaction products to examine the heterostructures and resultant optical properties.

Results and discussion

The product of the reaction between zinc stearate, InCl$_3$, and P(NMe$_2$)$_3$ displayed bright fluorescence prior to any surface deposition steps, as shown in Fig. 1. Note that the capping agents emitted a blue colour prior to quantum dot formation. Bare InZnP rarely displays PL due to the prevalence of surface trap states.[11,17,18,21,24,32] Fluorescence has been observed when carboxylates or zinc carboxylates were included in the synthesis with P(TMS)$_3$, but not previously with P(NMe$_2$)$_3$.[27,29,30] As shown in Fig. 1a–f, greater amounts of zinc stearate resulted in a shorter emission wavelength, with broad photoluminescence emission peaks of the crude aliquots suggesting heterogeneity in QD size or structure. For each Zn : In ratio, the emission red-shifted during the reaction, shown in Fig. 1g, indicating that the PL may originate from the ripening of alloyed QDs, rather than solely from trap or surface states. Emission emerged faster and at lower temperatures when less zinc stearate was present in the reaction. The emission spectra of In$_{[1]}$Zn$_{[0.5]}$P (Fig. 1a) are illustrative of this: the spectrum from time zero, when the reaction reached 220 °C, already displayed a clear emission peak at *ca.* 755 nm. Emission had therefore already developed at temperatures lower than this. In contrast, weak emission only emerged after two minutes at 220 °C in the synthesis of In$_{[1]}$Zn$_{[2.5]}$P, as shown in Fig. 1e. Zn : In ratios of 3 : 1 or greater did not produce detectable photoluminescence after 10 minutes at 220 °C (Fig. 1f). It is therefore possible that surface stearate groups controlled the formation, size, and growth rate of fluorescent nanoparticles.

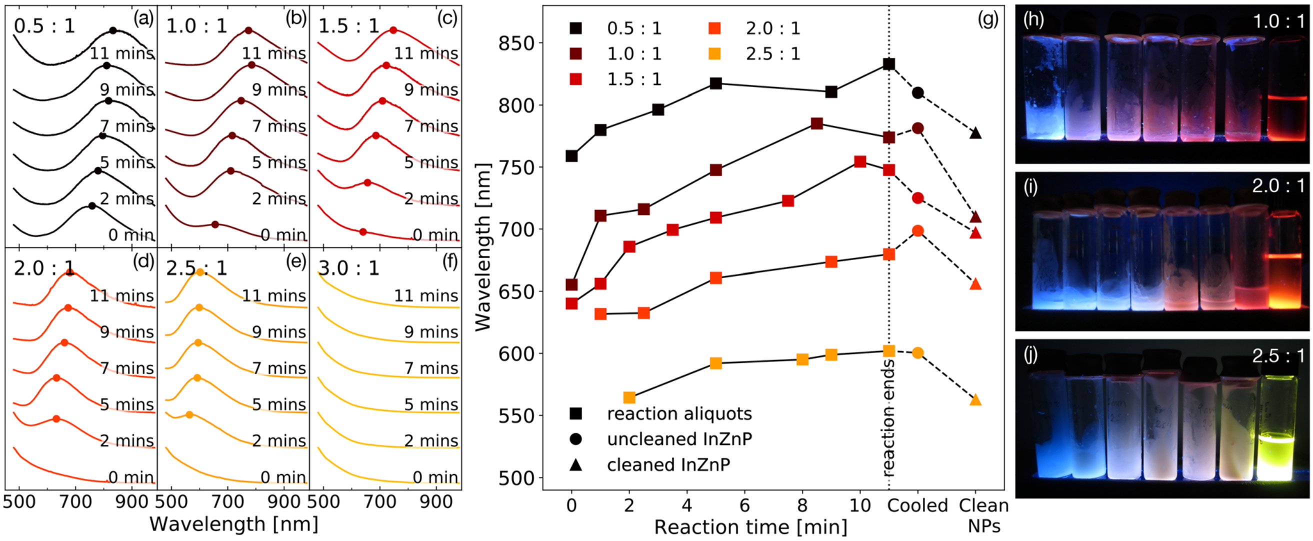

Fig. 1 a–f show the raw PL spectra of air-free aliquots removed at intervals during the synthesis of InZnP, with the Zn : In molar ratio indicated in the top left of each subplot. The emission peaks are broad and the PL wavelength is shorter the greater the Zn content. The PL peak wavelengths of the crude, air-free aliquots are plotted with square markers in g, showing a red-shift as the reaction progressed and a blue-shift with Zn : In ratio. The PL peak wavelength of the cooled, crude InZnP is plotted with a circle, and that of the cleaned, air-exposed product with a triangle. The emission blue-shifted on cleaning. h, i, and j show photos of the aliquots under 365 nm illumination for Zn : In ratios of 1.0 : 1, 2.0 : 1, and 2.5 : 1, respectively. The vials left-to-right are the progressive reaction aliquots, and the most right-hand vial is the cleaned product. Note the unreacted reagents emitted blue when excited at 365 nm.

Cooled samples of the reaction were exposed to air and cleaned. The photoluminescence emission wavelength of the cleaned product is plotted with a triangle in Fig. 1g and shows a clear blue shift relative to the crude product. This blue shift can arise from size focusing during cleaning, where larger QDs precipitate and smaller QDs remain suspended, or from surface modification during the cleaning procedure. The emission wavelength of the cleaned product was dependent on the Zn : In ratio, with PL peaks observed between 776 nm for cleaned $In_{[1]}Zn_{[0.5]}P$ and 566 nm for cleaned $In_{[1]}Zn_{[2.5]}P$ (Fig. 2a). The QY also increased with the Zn : In ratio, from only 0.6% for $In_{[1]}Zn_{[0.5]}P$, to 6.1% for $In_{[1]}Zn_{[2.0]}P$, and 15.1%

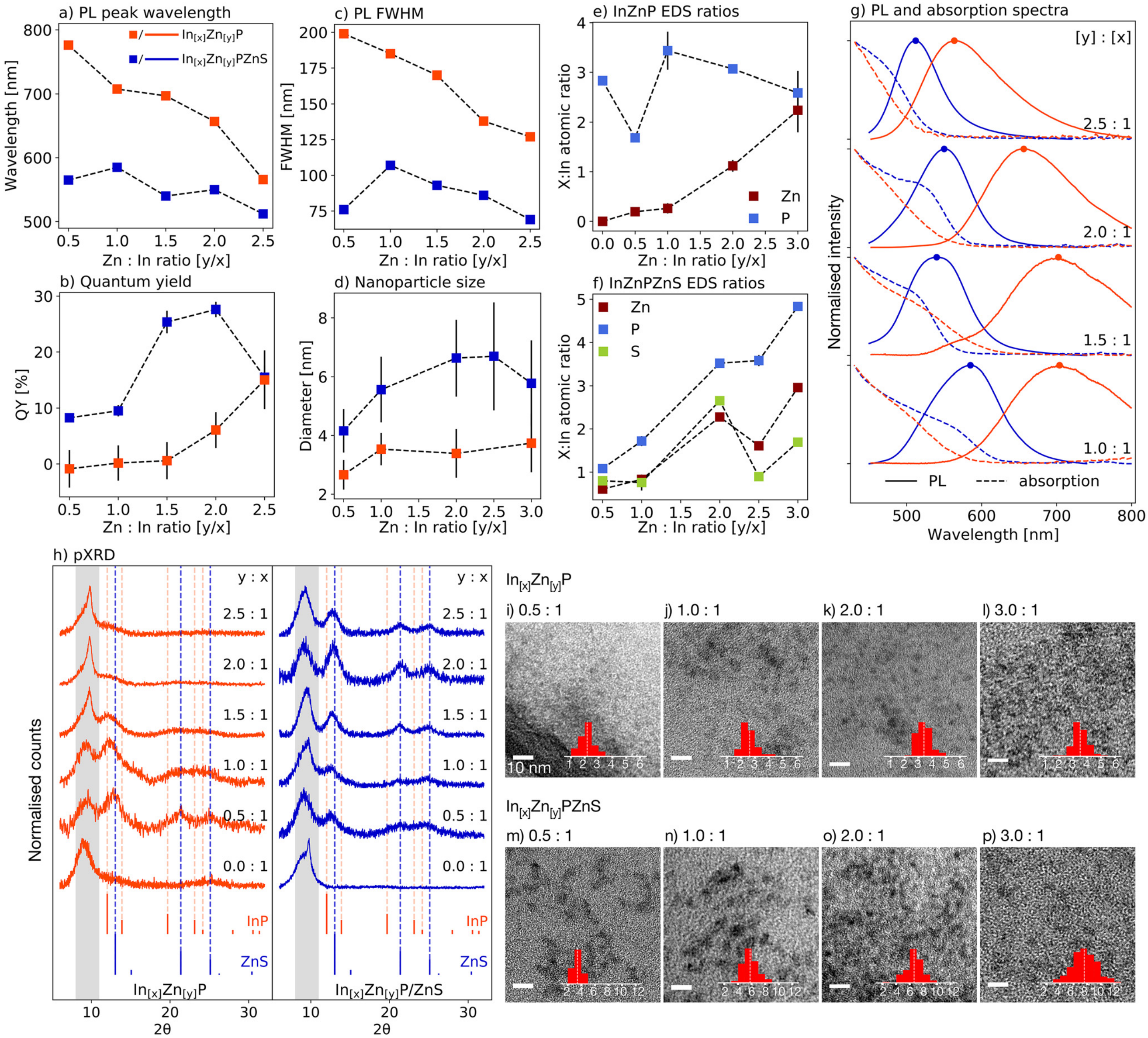

Fig. 2 a shows the peak PL wavelength of $In_{[x]}Zn_{[y]}P$ and $In_{[x]}Zn_{[y]}PZnS$ with Zn : In ratios from 0.5 : 1 to 2.5 : 1, with PL and absorption spectra shown in g. Samples synthesised without zinc stearate ("0.0 : 1") did not show detectable fluorescence; spectra for these materials are included in the ESI.† QYs are plotted in b, the PL FWHM in c, and d shows the mean nanoparticle diameters measured from electron microscopy images of at least thirty nanoparticles. The elemental compositions were measured with EDS and the atomic ratios normalised to In, as plotted in e ($In_{[x]}Zn_{[y]}P$) and f ($In_{[x]}Zn_{[y]}PZnS$). Error bars are the standard deviation of measurements. Powder XRD patterns of $In_{[x]}Zn_{[y]}P$ and $In_{[x]}Zn_{[y]}PZnS$, acquired using a Mo K_α (0.709 Å) source, are shown in h, along with reference patterns for InP and ZnS (PDF cards #00-032-0452,[37] #00-900-0107[38]). Broad diffraction patterns with similarity to InP were detected in $In_{[x]}Zn_{[y]}P$ when the Zn : In ratio used in synthesis was <2 : 1. The peaks were shifted to higher angles relative to pure InP, indicating contracted lattice dimensions due to alloying with Zn. A Bragg peak at 10° 2θ (highlighted in grey) was assigned to stearate-like ligands.[36] Patterns associated with cubic ZnS were present in all $In_{[x]}Zn_{[y]}PZnS$ samples except when zinc stearate was omitted from the core synthesis ("0.0 : 1"). The peak at 10° 2θ was maintained after ZnS surface deposition. TEM of $In_{[x]}Zn_{[y]}P$ and $In_{[x]}Zn_{[y]}PZnS$ nanoparticles with Zn : In ratios of 0.5 : 1 to 3.0 : 1 are shown in i–p with a histogram of the nanoparticle diameters inset in each image. Further EM images are available in the ESI.†

for $In_{[1]}Zn_{[2.5]}P$ (Fig. 2b). Furthermore, the emission linewidth (full width at half maximum, FWHM) narrows with increasing Zn : In ratio, dropping from 200 nm for $In_{[1]}Zn_{[0.5]}P$ to 130 nm for $In_{[1]}Zn_{[2.5]}P$ (Fig. 2c). While broad FWHMs can indicate heterogeneity in QD size or composition, recent work by Janke *et al.* also suggests that lattice disorder plays a significant role in broad InP emission profiles,[33] a theory further indicated by a Raman scattering study. The spectral acquisitions of InZnP with Zn : In ratios from 1 : 1 to 2 : 1 (ESI 2.2†) were characterized by broadened Raman features from 700 cm^{-1} onwards, consistent with the disordered Zn-doped InP measured by Janke *et al.*[33] Transverse and longitudinal optical modes (TO and LO) associated with InP were resolved for $In_{[1]}Zn_{[0.5]}P$ at 310 and 347 cm^{-1}, respectively, but observed only as a single broad scattering signal for Zn : In ratios of 1 : 1 and 2 : 1.[33] Broadening of the Raman scattering spectrum is associated with nanoscale materials[34] and lattice disorder arising from the incorporation of ionic Zn^{2+}.[33] The materials are therefore consistent with Zn-doped InP nanoparticles and an increasing degree of lattice disorder with the Zn : In ratio.

Three explanations for the optical shifts will be explored: first, that greater quantities of zinc stearate during synthesis resulted in smaller QDs. Second, that a graded structure or etched surface increased exciton confinement, resulting in blue-shifted PL. Third, that Zn-alloyed InP or a mixed amorphous structure formed, resulted in shorter bonding distances and blue-shifted PL, a phenomenon also observed by Thuy *et al.* in a synthesis with $PTMS_3$.[10] As shown in Fig. 2i–l, transmission electron microscopy (TEM) of the cleaned reaction product revealed the formation of small nanoparticles with diameters between 2.5 and 3.5 nm (Fig. 2d). There was no clear correlation between the QD size and the Zn : In ratio. Atomic ratios normalized to In were obtained by energy dispersive X-ray spectroscopy (EDS) and are shown in Fig. 2e, revealing a clear positive correlation between the Zn present in the product nanoparticles and the amount of zinc stearate included during synthesis. This supports the hypothesis that zinc stearate was a precursor to an alloyed or mixed amorphous InZnP, with the formation of this structure likely responsible for the blue-shift in optical properties (Fig. 2a–c and g).

$In_{[x]}Zn_{[y]}P$ QDs synthesised with various Zn : In ratios were characterized by powder X-ray diffraction (XRD) and the diffraction patterns plotted in Fig. 2h. Diffraction patterns with similarity to contracted cubic InP were observed for samples synthesised with Zn : In ratios of between 0.5 : 1 and 1.5 : 1, indicated the possible formation of alloyed InZnP.[10] The broad peaks were consistent with the small nanoparticles observed by TEM in Fig. 2i–l and comparable to those observed by Gu *et al.* for similar InZnP nanoparticles.[35] The Bragg peaks were weaker as a greater Zn : In ratio was used during synthesis. Samples synthesised with Zn : In ratios greater than 2.0 : 1 showed an absence of Bragg peaks, suggesting the presence of an amorphous semiconductor alloy, that there was significant disorder to any lattice structure, or that the particles were too small to be effectively detected by the diffractometer. As discussed previously, PL emission was also not observed for the samples with Zn : In ratios greater than 2.5 : 1, suggesting that photoluminescence was associated with the Zn-alloyed InP-like phase detected with XRD. A Bragg peak at 10° 2θ was detected in all samples and was likely associated with surface ligands, as observed recently by Calvin *et al.*[36] This feature at 10° was present regardless of the Zn : In ratio and sample fluorescence. No peaks associated with InP or InZnP were detected when zinc stearate was omitted from the synthesis (labeled "0.0 : 1" in Fig. 2h), suggesting that zinc stearate assisted the formation of alloyed InP-like QDs.

$In_{[1]}Zn_{[2.0]}P$ was chosen for detailed analysis due to its preferred optical properties in the red spectral region, and is named here as material **1**. High-angle annular dark field (HAADF) microscopy of **1**, in Fig. 3a, confirmed the presence of nanoparticles with diameters less than 4 nm. EDS mapping (Fig. 3b–d) revealed that Zn, In, and P were co-localised within these nanoparticles, further suggesting an alloyed structure. The lack of clear boundaries between individual nanoparticles in Fig. 3a–d indicates that organic surface species may be present, further suggested by the widespread prevalence of phosphorus between particles in Fig. 3d. Neither the sub-particle distribution of elements or the lattice structure could be resolved, either due to the sensitivity of the nanoparticles to the electron beam, or due to the presence of an amorphous or disordered structure.

Synchrotron-radiation (SR) excited X-ray photoelectron spectroscopy (XPS)[39] was used to study the depth-dependent composition of **1** prior to air-exposure, with the sampling depths for each photoelectron kinetic energy (KE) shown in Fig. 4a. The In 3d XP spectra, shown in Fig. 4c, displayed two distinct components. First, a feature with $3d_{5/2}$ binding energy (BE) of 445.4 eV, which was consistent with InP in a Zn-containing surround.[40] Second, a feature with $3d_{5/2}$ BE of 444.7 eV, which was consistent with pristine InP.[40] While the former was observed at all photoelectron (PE) sampling KEs, the latter was only observed at the higher (greater probing depths) photoelectron KEs of 550 and 800 eV, indicating a graded structure with more InP-like character in the centre of the nanoparticle and a greater Zn content on the surface. This structure was supported by the P 2p spectra, shown in Fig. 4d, which contained three components. First, a dominant peak with a P $2p_{3/2}$ BE of 129.0 eV, which was assigned to InP in a Zn-containing surround.[40] This feature shifted to 128.7 eV at higher photoelectron KEs, closer to the BE of pure InP, suggesting that the nanoparticle centre was more InP-like.[40] Second, a feature at 125.4 eV was observed, indicative of a phosphorus-containing organic material consistent with the precursors or capping agents observed by HAADF in Fig. 3d.[41] Third, a minor feature at 135.6 eV; this peak was assigned to phosphorous oxides, specifically P_2O_5 or P_4O_{10}.[42] These oxides are unusual in InP-based nanoparticles; $InPO_x$ species, with BE at *ca.* 133.5 eV, are more typically observed.[40] As plotted in Fig. 4e, the relative intensity of these oxide peaks increased at higher photoelectron KEs, suggesting that P_2O_5 or P_4O_{10} was more prevalent in the centre of the nanoparticle. These oxides

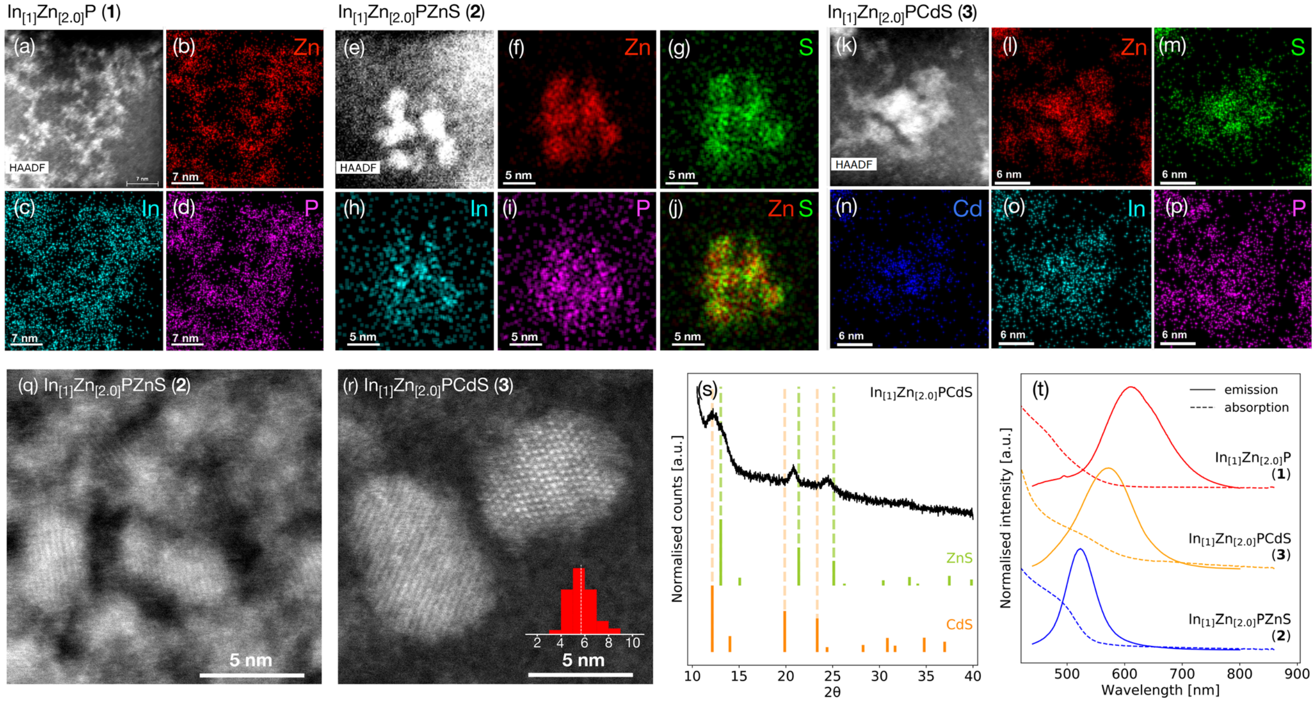

Fig. 3 Image a shows HAADF imaging of **1** ($In_{[1]}Zn_{[2.0]}P$); EDS maps of the same region are shown in b–d, identifying co-localisation of In, Zn, and P in the nanoparticles. The elemental structure could not be further resolved due to instability under the electron beam. Image e shows HAADF of **2** ($In_{[1]}Zn_{[2.0]}PZnS$); EDS maps of the same region are shown in f–i, and a composite of the Zn and S maps are in j. Image k shows HAADF of **3** ($In_{[1]}Zn_{[2.0]}PCdS$); EDS maps of the same region are shown in l–p. No core/shell structure was observed for either **2** or **3**, suggesting an alloyed material. **2** and **3** were crystalline, with lattice fringes clearly observed in q and r. XRD of **3**, acquired using a Mo K_α (0.709 Å) source, is shown in s, along with the reference patterns for ZnS (PDF card 00-900-0107) and CdS (PDF card 00-101-1251). PL and absorption spectra for **1**, **2**, and **3** are shown in t.

therefore likely formed during synthesis rather than from post-synthesis oxidation. Given the particles were synthesised and processed for XPS in air-free conditions, it is probable that the carboxylate group of zinc stearate was the source of these oxides, a similar finding to that of Virieux *et al.*[40]

Only one feature was observed in the Zn 2p spectrum (included in the ESI†), suggesting a single bonding environment throughout the nanoparticle. The $2p_{3/2}$ BE of 1020.6 eV was consistent with Zn–P bonding,[43,44] confirming the presence of Zn within the nanoparticle structure and the formation of an InZnP alloy. However, the BEs of ZnP_2 (1020.9 eV)[44] and Zn_3P_2 (1020.6 eV)[43] are too similar for this peak to be conclusively assigned. As shown in Fig. 4f, Zn 2p spectra were obtained up to sampling depths of 1.44 nm; with total nanoparticle diameters in the region of only 3.4 nm, this confirms that Zn was incorporated throughout most of the structure.

The Zn 2p, P 2p, and In 3d XP spectra therefore confirmed the presence of an alloyed InZnP structure: the Zn 2p spectrum confirms the existence of Zn–P bonding, while the P 2p and In 3d spectra confirm the presence of InP in a Zn-containing environment. Zinc stearate therefore behaved as a zinc precursor in this study.

The total peak areas of the P and Zn XP spectra were normalised to In 3d to reveal the depth-dependent elemental compositions, as shown in Fig. 4f. Zn had greater prevalence on the nanoparticle surface, indicating a graded alloyed structure and suggesting the presence of zinc carboxylate as a surface species. The Zn-rich nanoparticle surface may account for the PL displayed by the particles prior to exposure to air. As proposed by Ryu *et al.*,[27] Zn can passivate InP surface trap states and improve radiative recombination. However, the presence of oxidised P-containing species within the nanoparticle may also result in weak PL, as observed by Buffard *et al.*[18] Oxide-associated trap states typically result in PL QYs of *ca.* 1%, much lower than the 6.1% observed for material **1**, suggesting that surface passivation by Zn is more likely responsible for the observed PL. One interesting possibility is the potential for a InP/ZnO layer to have formed,[45] which is further endorsed by the presence of ZnO binding energies, as will be discussed later.

To characterise the chemical changes that occurred following exposure to air, XPS of **1** was also obtained in atmospheric conditions using a monochromatic X-ray source. As shown in Fig. 5a, oxidised material consistent with $InPO_x$ was dominant in the P 2p XP spectrum. $InPO_x$ species are commonly observed in InP-based materials, including in recent studies by Vikram *et al.* in which they formed on the InP surface and at the core/shell interface of InP/ZnSe.[46] No features consistent with P_2O_5 or P_4O_{10} were observed, unlike the air-free samples in Fig. 4. The total $P_{ox} : P_{InP}$ ratio was 3.8 : 1, compared to 0.01 : 1 measured by SR-XPS on the nanoparticle surface prior to air exposure. Air-exposed samples displayed a Zn $3p_{3/2}$ BE of 89.2

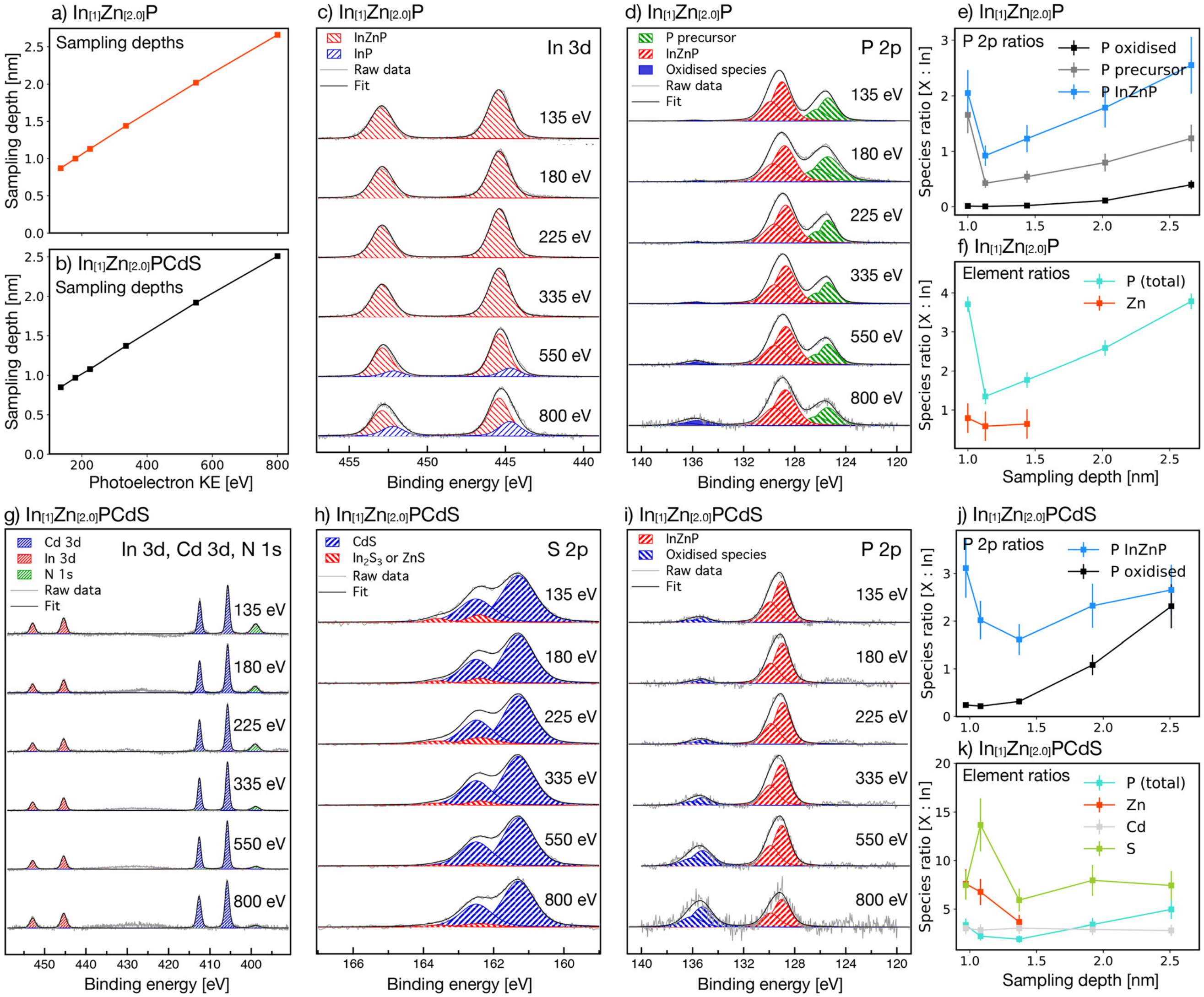

Fig. 4 Synchrotron radiation-excited depth-profiling XP spectra. Plots a and b show the sampling depths through the nanoparticles at each photoelectron KE. Plot c shows normalised SR-XP spectra of the In 3d orbitals in $In_{[1]}Zn_{[2.0]}P$ (**1**) with photoelectron sampling KEs from 135 to 800 eV. Two bonding environments were observed: InP in a zinc-containing surround (InZnP), and pristine InP. Plot d shows SR-XP spectra of P 2p orbitals with three bonding environments observed: InZnP-like peaks, precursor-related species, and oxidised species. The ratios of the P bonding environments normalised to In 3d are shown in plot e. The total elemental ratios of P and Zn relative to In are shown in plot f. Plot g shows the normalised SR-XP spectra for In 3d, Cd 3d, and N 1s in $In_{[1]}Zn_{[2.0]}PCdS$ (**3**), with a single bonding environment observed for each. Plot h shows the normalised SR-XP spectra of S 2p orbitals in **3**, with bonding environments associated with CdS and ZnS or In_2S_3. Plot i shows the P 2p SR-XP spectra for in **3**, revealing two bonding environments, one associated with InP in a zinc-containing surround (InZnP) and one with oxidised P-containing species. The ratios of P bonding environments within **3**, normalised to In 3d, are shown in plot j. The total elemental ratios of P, Zn, and Cd relative to In 3d within **3** are shown in plot k.

eV, while the Zn 3s BE in Fig. 5 was 140.2 eV. Both these BEs were higher than would typically be observed for ZnP_2 or Zn_3P_2[43,44] and more consistent with ZnO.[47,48] The Zn-containing surface therefore did not prevent widespread oxidation of the nanoparticles.

InZnP QDs with Zn : In ratios from 0.5 : 1 to 3.0 : 1 were heated to 300 °C with zinc diethyldithiocarbamate (ZDEC), a single-source ZnS precursor, forming $In_{[x]}Zn_{[y]}PZnS$ nanoparticles (we omit the usual nomenclature of 'InP/ZnS' and adopt the description previously used by Reiss for alloyed InPZnS prepared in a one pot reaction, putting the order of elements from the centre of the particles outwards[13]). TEM revealed no clear correlation between the core Zn : In ratio and the nanoparticle diameters, as shown in Fig. 2d. For example, $In_{[1]}Zn_{[1.0]}PZnS$, $In_{[1]}Zn_{[2.0]}PZnS$, and $In_{[1]}Zn_{[3.0]}PZnS$ had average diameters of 5.8 ± 1.1, 6.6 ± 1.3, and 5.8 ± 1.4 nm, respectively, with mean and standard deviation calculated from a sample of at least 30 particles. The diameters of $In_{[x]}Zn_{[y]}PZnS$ were on average 2.4 nm greater than the core InZnP nanoparticle, equivalent to 3–4 monolayers of ZnS,[49] confirming that ripening or surface deposition occurred during the reaction with ZDEC.

Elemental compositions for $In_{[y]}Zn_{[x]}PZnS$ with different core Zn : In ratios were calculated from EDS and are shown in

Fig. 2f. There was not a strong correlation between the S : In ratio of the shelled materials and the core Zn : In ratio, with an average S : In ratio across all samples of 1.36 ± 0.73. However, the P : In and Zn : In ratios of $In_{[y]}Zn_{[x]}PZnS$ were more clearly correlated with the core zinc content. For example, the Zn : In ratios of $In_{[1]}Zn_{[3.0]}PZnS$ and $In_{[1]}Zn_{[0.5]}PZnS$ were 3.0 : 1 and 0.6 : 1, respectively, initially suggesting that the internal InZnP structure was maintained after the ZnS deposition procedure.

X-ray diffraction studies, shown in Fig. 2h, confirmed the formation of a cubic ZnS-like phase on InZnP nanoparticles with all Zn : In ratios, but not on the amorphous "$In_{[1]}Zn_{[0.0]}P$" material that formed when zinc stearate was omitted from the core synthesis. The Bragg peak previously observed at *ca.* 10° 2θ in all InZnP samples, assigned to surface stearate ligands, broadened and shifted to lower diffraction angles following the surface deposition of ZnS. This indicated a change to the surface structure of the nanoparticles.

The optical properties of $In_{[x]}Zn_{[y]}PZnS$ suggest that deposition of ZnS passivated trap sites on InZnP and improved crystallinity. As shown in Fig. 2b, $In_{[x]}Zn_{[y]}PZnS$ nanoparticles displayed significantly brighter fluorescence than the respective core materials, with a maximum QY of 27% observed for $In_{[1]}Zn_{[2.0]}PZnS$ compared to 6.1% for $In_{[1]}Zn_{[2.0]}P$. Furthermore, all $In_{[x]}Zn_{[y]}PZnS$ nanoparticles displayed clear band-edge excitonic absorption features in Fig. 2g, in contrast to $In_{[x]}Zn_{[y]}P$ which had absorbance more typical of an amorphous material. Likewise, the emission FWHM of $In_{[x]}Zn_{[y]}PZnS$ was consistently narrower than that of the parent $In_{[x]}Zn_{[y]}P$ (Fig. 2c), suggesting greater homogeneity in nanoparticle size and structure and reduction in trapping states. The FWHM was narrower for $In_{[x]}Zn_{[y]}PZnS$ nanoparticles with greater core Zn : In ratios, reducing from 107 nm for $In_{[1]}Zn_{[1.0]}PZnS$ to 69 nm for $In_{[1]}Zn_{[2.5]}PZnS$.[10]

The photoluminescence wavelengths of $In_{[x]}Zn_{[y]}PZnS$ nanoparticles were consistently blue-shifted by approximately 60 nm relative to the $In_{[x]}Zn_{[y]}P$ cores (Fig. 2a), indicating an increased band-gap energy following surface deposition of ZnS. However, the overall nanoparticle diameter increased following ZnS deposition (Fig. 2d): this blue-shift did not originate from simple quantum confinement. Two alternative explanations will be examined: first, that ZnS alloyed into the InZnP core, reducing the effective core diameter and increasing the exciton confinement. Second, that alloying of Zn^{2+} into InZnP reduced the interatomic distances and raised the exciton energy, an effect observed by Thuy *et al.* on the formation of graded InP/ZnS.[10]

The presence of more zinc stearate during the core synthesis resulted in shorter emission wavelengths for $In_{[x]}Zn_{[y]}PZnS$ (Fig. 2g), similar to the trend observed for $In_{[x]}Zn_{[y]}P$. This indicates that ZnS deposition occurred on $In_{[x]}Zn_{[y]}P$, rather than the formation of a separate population of ZnS nanoparticles.

$In_{[1]}Zn_{[2.0]}PZnS$, the product of the reaction between **1** and ZDEC, was chosen for further structural analysis and is henceforth named **2**. HAADF of **2** (Fig. 3e) confirmed the formation of crystalline nanoparticles: clear lattice fringes were observed with high-resolution STEM (Fig. 3q). The lattice separation was 0.31 ± 0.2 nm, consistent with the {111} plane of zinc blende ZnS,[50] indicating that the exterior of **2** was principally ZnS-like. EDS mapping (Fig. 3f–j) revealed that that In, P, Zn, and S were co-localised within the nanoparticles, further confirming that Zn and S deposited onto InZnP. A core/shell structure could not be resolved, suggesting that ZnS did not necessarily form a discrete surface phase.

XP spectra of **2** (Fig. 5d–f) confirmed the formation of ZnS: the BE of the S $2p_{3/2}$ peak was 161.7 eV, consistent with ZnS-like bonding.[51] Further alloying occurred during the ZnS deposition: InP-associated P 2p peaks had a lower prevalence in **2** than **1** (Fig. 5d), suggesting that the InP-like centre present in **1** was eradicated during shell deposition. However, as discussed earlier and shown in Fig. 2, the shelled materials maintained the properties of the core, including elemental composition and optical trends.

CdS was deposited onto the surface of **1** using cadmium diethyldithiocarbamate (CDEC), the Cd analogue of ZDEC, resulting in $In_{[1]}Zn_{[2.0]}PCdS$ (material **3**). Annular dark-field imaging (Fig. 3r) revealed crystalline ovoid QDs with an average length of 5.7 ± 1.0 nm and lattice spacings of 0.33 ± 0.1 nm; this value is midway between the {111} *d*-spacings of pure cubic ZnS (0.312 nm) and CdS (0.336 nm),[50] suggesting that surface of **3** was a ZnCdS alloy. This alloyed structure was also indicated by XRD in Fig. 3s: the diffraction peaks for **3** revealed a cubic zinc blende structure with lattice spacings between ZnS and CdS.

Elemental mapping of **3**, in Fig. 3l–p, confirmed that Zn, In, P, S, and Cd were co-localised within the nanoparticles. The atomic composition was measured from EDS and normalised to In, revealing a relative composition $In_{1.0}Zn_{5.2}P_{1.8}Cd_{0.9}S_{2.3}$, compared to $In_{1.0}Zn_{0.5}P_{1.1}$ for **1** and $In_{1.0}Zn_{6.5}P_{1.7}S_{4.5}$ for **2**. Material **3** therefore had a greater total Zn and P content than **1**, despite CDEC containing neither of those elements. We suggest that residual zinc stearate and $P(NMe_2)_3$ continued to react during the surface deposition procedure, further indicating that zinc stearate behaved as a precursor. **3** was stable under the electron beam and clearly crystalline, but separate core/shell phases could not be resolved. This suggested an alloyed structure, consistent with XRD and the observed lattice spacings.

The optical properties of **3** were largely intermediate between those of **1** and **2**. For example, the emission wavelength was 570 nm (Fig. 3t), compared to 660 and 550 nm for **1** and **2**, respectively. Similarly, **3** had a FWHM of 104 nm and a Stokes' shift of 66 nm; in both cases, larger than **2** yet smaller than **1**. Peter *et al.* suggest that the band-gap of a ZnCdS alloy increases with Zn content, becoming more ZnS-like, and decreases with Cd content, becoming more CdS-like.[52] The ZnCdS-like structure of **3** may therefore result in a narrower band-gap than the more ZnS-like **2**, accounting for the observed optical properties. The QY of **3** was 36%, significantly higher than either **2** or **1** (27% and 6%, respectively), suggesting improved passivation of trap states from CdS surface deposition.

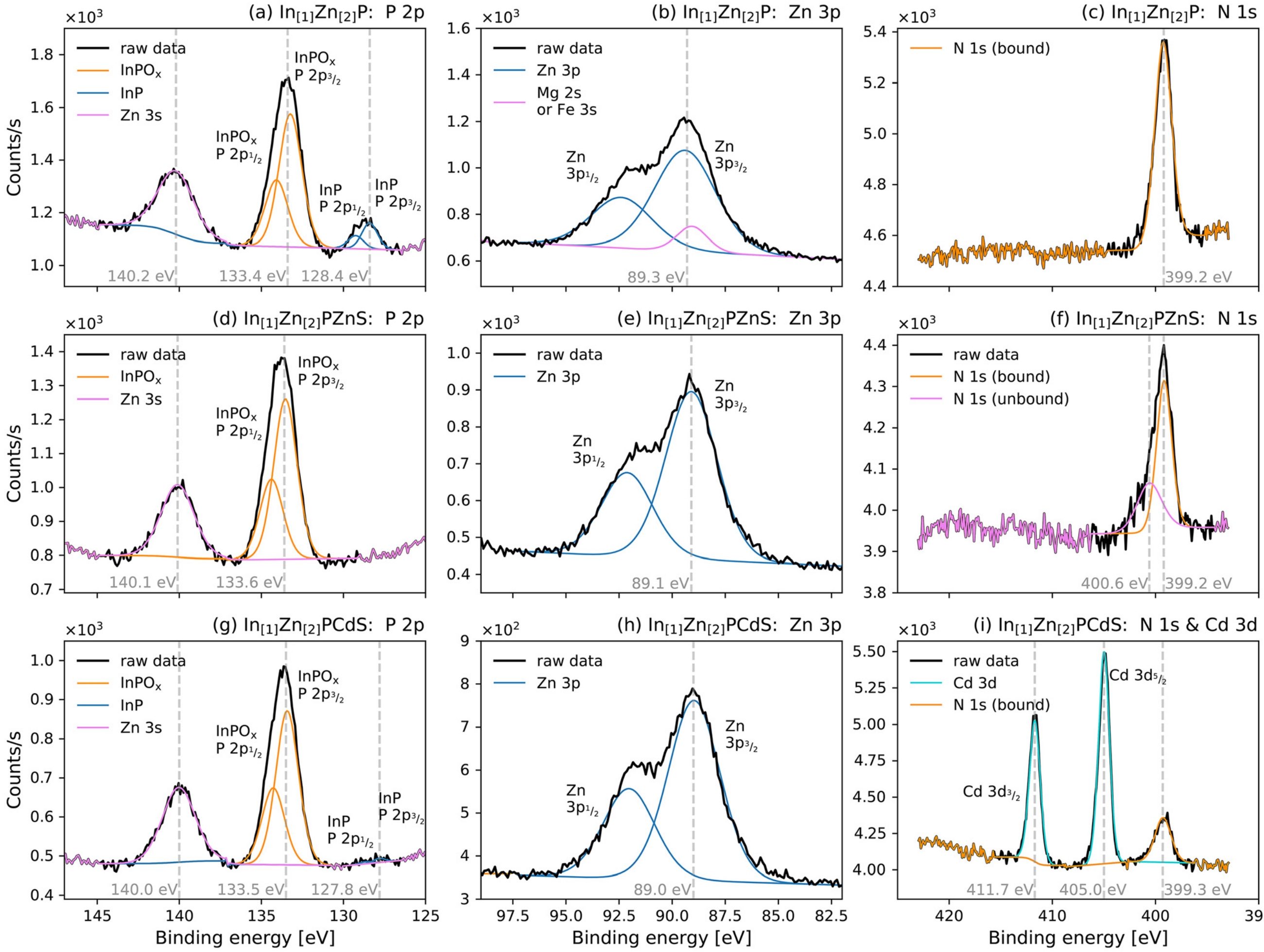

Fig. 5 XP spectra of air-exposed samples of $In_{[1]}Zn_{[2]}P$ (**1**) in subplots a, b, and c; $In_{[1]}Zn_{[2]}PZnS$ (**2**) in subplots d, e, and f; and $In_{[1]}Zn_{[2]}PCdS$ (**3**) in subplots g, h, and i. Spectra associated with P 2p and Zn 3s orbitals are in a, d, and g; a strong signal from oxidised $InPO_x$ was detected in all samples. This indicates further oxidation compared to the P_2O_5 or P_4O_{10} species detected in the air-free samples in Fig. 4e and f. InP species were also detected in samples of **1** and **3**. Spectra associated with Zn 2p orbitals are in b, e, and h. Spectra associated with N 1s and Cd 3d orbitals are in c, f, and i. No species associated with Cd 3d were detected in either **1** or **2**, but Cd $3d_{5/2}$ orbitals with BE 405.0 eV, consistent with CdS, were observed in **3**.

Without prior exposure to air, SR-excited depth-profiling XP spectra were measured for **3** and are shown in Fig. 4g–i. The correlation between photoelectron KE and sampling depth is plotted in Fig. 4b, and the ratios of individual species normalised to In 3d are in Fig. 4j and k. The In $3d_{5/2,\ 3/2}$ and Cd $3d_{5/2,\ 3/2}$ XP spectra (Fig. 4g) both had one feature at all sampling depths, suggesting a single bonding environment throughout the entirety of the nanoparticles. The In $3d_{5/2}$ peak was located at 445.4 eV, the same BE as in **1**; the presence of Cd and S did not significantly change the bonding environment of In. This peak could be assigned to either InP in a Zn-containing surround[40] or to In_2S_3,[53,54] so firm conclusions could not be drawn as to its structural origin. Unlike **1**, no peaks associated with pristine InP were detected at any photoelectron KEs in the In $3d_{5/2,\ 3/2}$ spectra: the prolonged reaction with CDEC enabled the diffusion of Zn into the centre of the nanoparticle. A single component was observed in the Zn 2p spectra of **3** (included in the ESI†). However, the bonding environment around Zn could not be identified because the $2p_{3/2}$ BE of 1020.6 eV could be assigned to either ZnS[51,55] or Zn_3P_2.[43] The presence of only one Zn 2p component for all photoelectron KEs confirmed that Zn was homogeneously alloyed throughout **3**.

In contrast, the S $2p_{3/2}$ spectra had two distinct features (Fig. 4h). First, a dominant peak with BE 161.7 eV, which was consistent with CdS.[56,57] Second, a minor peak was at 162.9 eV, which could be assigned to either ZnS[51,58] or In_2S_3.[53,54] This latter peak was more intense at lower photoelectron KEs, suggesting that ZnS and/or In_2S_3 were more prevalent in the outer regions of the nanoparticle. Given the presence of both a CdS-associated peak and a ZnS-associated peak in the lowest photoelectron KE spectra, it is likely that the surface was a ZnCdS alloy. This corroborates the findings of both XRD and STEM, which identified a lattice structure with dimensions between that of ZnS and CdS. This was further indicated by the Cd 3d spectra (Fig. 4g): the binding energy of Cd $3d_{5/2}$ was 405.1 eV, consistent with a CdS-like material.[56,57]

The peak areas for the constituent species were normalised to In 3d to approximate the depth-dependent composition (Fig. 4k). The Cd : In ratio remained constant across all sampling depths, suggesting that Cd was homogeneously distributed throughout **3** and that a more typical InP/CdS core/shell structure was not formed.[59,60] The relative Zn concentration decreased with increasing photoelectron KE, suggesting that the outer regions of **3** were Zn-rich. For example, the In : Zn ratios were 1.0 : 7.6 and 1.0 : 3.7 at sampling depths of 0.97 and 1.08 nm, respectively, suggesting an alloyed structure with a significant drop in Zn concentration towards the nanoparticle centre. The S $2p_{3/2}$ peak at 162.9 eV, which was consistent with either ZnS or In_2S_3, was also more prevalent in the outer regions of **3**. The greater concentration of Zn in this same region further suggests that ZnS is a more likely candidate than In_2S_3. However, the overall S : In ratio was relatively constant throughout the nanoparticles, and the CdS-associated peaks were present at all sampling depths. These findings strongly indicate that the surface of **3** was a Zn-rich ZnCdS alloy, with Cd and S additionally alloyed throughout the QDs with uniform distribution. This CdS-like structure was also confirmed by monochromatic-radiation XPS, with the Cd 3d spectrum in Fig. 5i.

The Zn : In ratio of **3** was approximately ten times greater than **1** across all available sampling depths, as shown by comparing Fig. 4f and k, respectively. No additional zinc precursors were added during the CdS deposition procedure, confirming that zinc stearate behaved as a precursor to produce an alloyed material. However, additional oxidation also occurred during the reaction with CDEC, as shown by the P 2p spectra in Fig. 4i. Two $2p_{3/2}$ features, at 129.0 and 135.2 eV, were associated with InZnP[40] and oxidised species,[42] respectively. Similar to **1**, the oxide species were more prevalent at greater photoelectron KEs, consistent with a more oxidised core (Fig. 4j). For example, the normalised ratio of $P_{InZnP} : P_{ox}$ was 1 : 0.87 at sampling depths of 2.51 nm, compared to only 1 : 0.08 at 0.97 nm. The oxide : In ratio was also significantly higher in **3** than **1** (Fig. 4j and e, respectively). As discussed previously, zinc stearate continued to react during the CdS deposition procedure, resulting in Zn diffusion throughout the nanoparticle. The stearate group may also be the cause of additional oxidation, similar to the mechanism proposed by Virieux *et al.*, in which carboxylates oxidise InP during synthesis.[40] It is also possible that air was introduced to the reaction vessel during injection of CDEC, although this effect is likely minimal due to the air-free syringes and positive nitrogen pressure that were used throughout.

Conclusions

Fluorescent InZnP nanoparticles were synthesised in a simple one-pot reaction using a relatively safe and green phosphorous precursor. The emission wavelength was tuned from 566 to 776 nm by varying the Zn : In molar ratio during synthesis. The maximum QY was 15%, an unusually high value for bare InP-based nanoparticles without a shell or etched surface. Zinc stearate was found to be a true precursor, resulting in alloyed InZnP, unlike previous studies with zinc halides and $P(NMe_2)_3$ in which Zn was merely a spectator ion.[11,18] Kirkwood *et al.* have recently reported that InZnP quantum dots synthesised with zinc carboxylates and $PTMS_3$ have an alloyed structure with Zn primarily located at the surface, although some Zn was also found deeper in the particles.[28] The InZnP nanoparticles presented here, produced with $P(NMe_2)_3$ and zinc carboxylates, had a similar Zn-rich surface but also appeared to have a significant Zn content in the centre of the nanoparticles. Notably, phosphorous oxides in the form P_2O_5 or P_4O_{10} were also observed at the centre of InZnP following the air-free synthesis. $InPO_x$ species were observed in all materials that were exposed to air, similar to recent structural studies by Vikram *et al.*[46] However, this extensive oxidation did not quench the fluorescence, and air-exposed materials maintained similar optical properties to the air-free aliquots.

Alloyed InZnPZnS nanoparticles were formed following a surface deposition procedure with ZDEC. The optical properties of InZnPZnS were dependent on the core InZnP, showing that ZnS deposited on and modified the original InZnP materials but did not totally eradicate their structure. The surface deposition of CdS using CDEC resulted in alloyed InZnPCdS with a QY of 36%. Structural studies indicated that Cd, In, P, and S were largely homogeneously alloyed, whilst Zn was more prevalent on the nanoparticle surface, suggesting a graded material with a Zn-rich ZnCdS surface. Zinc stearate continued to react during the one-pot shell deposition procedure, further cementing its role as a precursor.

It is noteworthy that the diethyldithiocarbamate shelling precursors resulted in alloying throughout the entire nanoparticle, not just at the core/shell interface. This study also highlights the ease with which Zn alloys through InP-type nanoparticles. These findings highlight the broad and complex range of potential structures available to the III–V family of materials. Elemental analysis often cannot reveal this internal structure, unlike depth-profiling SR-excited XPS, utilised in this study. While many similar reactions are superficially described as producing core/shell systems, differing structures will result from the complex range of variables, including precursors, reaction conditions, capping agents, and solvents. In this study, the nomenclature 'InP/ZnS' or 'InP/CdS' is too simplistic to describe the end products, which displayed extensive alloying. While the surface deposition had a passivating effect, including increasing the QY, distinct core and shell phases were not formed. These materials would benefit from additional studies into the electronic structure to fully realise their potential and elucidate their exact structures. It is worth noting that a recent study by Sun *et al.* has described the inhibition of the cation exchange at the core/shell interface to obtain brightly emitting InP/ZnSe/ZnS quantum dots, by introducing a Se-rich shielding layer between core and first shell, exhibiting emission quantum yields of up to 87%.[61]

Abbreviations

1	$In_{[1]}Zn_{[2.0]}P$
2	$In_{[1]}Zn_{[2.0]}PZnS$
3	$In_{[1]}Zn_{[2.0]}PCdS$
CDEC	Cadmium diethyldithiocarbamate
EDS	Energy dispersive X-ray spectroscopy
FWHM	Full width at half maximum
PL	Photoluminescence
$PTMS_3$	Tris(trimethylsilyl)phosphine
QD	Quantum dot
SR	Synchrotron radiation-excited
XPS	X-ray photoelectron spectroscopy
ZDEC	Zinc diethyldithiocarbamate

Conflicts of interest

There are no conflicts to declare.

Acknowledgements

We acknowledge fund *via* the Engineering and Physical Sciences Research council (EPSRC) for partial funding of this project (EP/M015653/1, EP/M015513/2). Thanks to L. Glover at the Centre for Ultrastructural Imaging for assistance with TEM.

References

1 K. T. Yong, *et al.*, Imaging Pancreatic Cancer Using Bioconjugated InP Quantum Dots, *ACS Nano*, 2009, **3**(3), 502–510.

2 S. Hussain, *et al.*, One-Pot Fabrication of High-Quality InP/ZnS (Core/Shell) Quantum Dots and Their Application to Cellular Imaging, *ChemPhysChem*, 2009, **10**(9–10), 1466–1470.

3 L. Zhang, *et al.*, In vivo tumor active cancer targeting and CT-fluorescence dual-modal imaging with nanoprobe based on gold nanorods and InP/ZnS quantum dots, *J. Mater. Chem. B*, 2018, **6**, 2574–2583.

4 S. Gao, *et al.*, Lasing from colloidal InP/ZnS quantum dots, *Opt. Express*, 2011, **19**(6), 5528–5535.

5 S. Shutts, *et al.*, Exploring the wavelength range of InP/AlGaInP QDs and application to dual-state lasing, *Semicond. Sci. Technol.*, 2015, **30**(4), 044002.

6 T. Fukuda and H. Sasaki, Improvement in luminance of light-emitting diode using InP/ZnS quantum dot with 1-dodecanethiol ligand, *Jpn. J. Appl. Phys.*, 2018, **57**(3S2), 03EH06.

7 X. Yang, *et al.*, Full Visible Range Covering InP/ZnS Nanocrystals with High Photometric Performance and Their Application to White Quantum Dot Light-Emitting Diodes, *Adv. Mater.*, 2012, **24**(30), 4180–4185.

8 S. J. Yang, *et al.*, Realization of InP/ZnS quantum dots for green, amber and red down-converted LEDs and their color-tunable, four-package white LEDs, *J. Mater. Chem. C*, 2015, **3**, 3582–3591.

9 M. J. Anc, *et al.*, Progress in Non-Cd Quantum Dot Development for Lighting Applications, *ECS J. Solid State Sci. Technol.*, 2013, **2**(2), R3071–R3082.

10 U. T. D. Thuy, P. Reiss and N. Q. Liem, Luminescence properties of In(Zn)P alloy core/ZnS shell quantum dots, *Appl. Phys. Lett.*, 2010, **97**, 193104.

11 M. D. Tessier, *et al.*, Economic and Size-Tunable Synthesis of InP/ZnE (E=S, Se) Colloidal Quantum Dots, *Chem. Mater.*, 2015, **27**(13), 4893–4898.

12 S. M. Joung, *et al.*, Facile synthesis of uniform large-sized InP nanocrystal quantum dots using tris(tert-butyldimethylsilyl)phosphine, *Nanoscale Res. Lett.*, 2012, **7**(1), 93.

13 L. Li and P. Reiss, One-pot Synthesis of Highly Luminescent InP/ZnS Nanocrystals without Precursor Injection, *J. Am. Chem. Soc.*, 2008, **130**(35), 11588–11589.

14 O. I. Micic, *et al.*, Synthesis and Characterization of InP Quantum Dots, *J. Phys. Chem.*, 1994, **98**(19), 4966–4969.

15 K. Huang, *et al.*, Internal Structure of InP/ZnS Nanocrystals Unraveled by High-Resolution Soft X-ray Photoelectron Spectroscopy, *ACS Nano*, 2010, **4**(8), 4799–4805.

16 P. Mushonga, *et al.*, One-pot synthesis and characterization of InP/ZnSe semiconductor nanocrystals, *Mater. Lett.*, 2013, **95**, 37–93.

17 D. C. Gary, B. A. Glassy and B. M. Cossairt, Investigation of Indium Phosphide Quantum Dot Nucleation and Growth Utilizing Triarylsilylphosphine Precursors, *Chem. Mater.*, 2014, **26**(4), 1734–1744.

18 A. Buffard, *et al.*, Mechanistic Insight and Optimization of InP Nanocrystals Synthesized with Aminophosphines, *Chem. Mater.*, 2016, **28**(16), 5925–5934.

19 H.-J. Byun, W.-S. Song and H. Yang, Facile consecutive solvothermal growth of highly fluorescent InP/ZnS core/shell quantum dots using a safer phosphorus source, *Nanotechnology*, 2011, **22**(23), 235605.

20 W.-S. Song, *et al.*, Amine-derived synthetic approach to color-tunable InP/ZnS quantum dots with high fluorescent qualities, *J. Nanopart. Res.*, 2013, **15**(6), 1–10.

21 M. D. Tessier, *et al.*, Aminophosphines: A Double Role in the Synthesis of Colloidal Indium Phosphide Quantum Dots, *J. Am. Chem. Soc.*, 2016, **138**(18), 27111735.

22 J.-H. Jo, *et al.*, InP-Based Quantum Dots Having an InP Core, Composition-Gradient ZnSeS Inner Shell, and ZnS Outer Shell with Sharp, Bright Emissivity, and Blue Absorptivity for Display Devices, *ACS Appl. Nano Mater.*, 2020, **3**(2), 1972–1980.

23 U. T. D. Thuy, *et al.*, Europium doped In(Zn)P/ZnS colloidal quantum dots, *Dalton Trans.*, 2013, **42**, 12606–12610.

24 W. Yang, *et al.*, Surface passivation extends single and biexciton lifetimes of InP quantum dots, *Chem. Sci.*, 2020, **11**, 5779–5789, s.l., RSC.

25 S. Tamang, *et al.*, Chemistry of InP Nanocrystal Syntheses, *Chem. Mater.*, 2016, **28**(8), 2491–2506.

26 J. I. Kim and J. K. Lee, Sub-kilogram-Scale One-Pot Synthesis of Highly Luminescent and Monodisperse Core/

Shell Quantum Dots by the Successive Injection of Precursors, *Adv. Funct. Mater.*, 2006, **16**(16), 2077–2082.

27 E. Ryu, *et al.*, Step-Wise Synthesis of InP/ZnS Core-Shell Quantum Dots and the Role of Zinc Acetate, *Chem. Mater.*, 2009, **21**(4), 573–575.

28 N. Kirkwood, *et al.*, Locating and Controlling the Zn Content in In(Zn)P Quantum Dots, *Chem. Mater.*, 2020, **32**(1), 557–565.

29 S. Xu, J. Ziegler and T. Nann, Rapid synthesis of highly luminescent InP and InP/ZnS nanocrystals, *J. Mater. Chem.*, 2008, **18**, 2653–2656.

30 S. Xu, *et al.*, Optical and Surface Characterisation of Capping Ligands in the Preparation of InP/ZnS Quantum Dots, *Sci. Adv. Mater.*, 2009, **1**(2), 125–137.

31 J. J. Calvin, *et al.*, Thermodynamic investigation of increased luminescence in indium phosphide quantum dots by treatment with metal halide salts, *J. Am. Chem. Soc.*, 2020, **142**(44), 18897–18906.

32 F. Zan and J. Ren, Gas-liquid phase synthesis of highly luminescent InP/ZnS core/shell quantum dots using zinc phosphide as a new phosphorus source, *J. Mater. Chem.*, 2012, **22**, 1794–1799.

33 E. M. Janke, *et al.*, Origin of Broad Emission Spectra in InP Quantum Dots: Contributions from Structural and Electronic Disorder, *J. Am. Chem. Soc.*, 2018, **140**(46), 15791–15803.

34 M. J. Seong, *et al.*, Size-dependent Raman study of InP quantum dots, *Appl. Phys. Lett.*, 2003, **82**, 185–187.

35 H. Gu and J. Zhang, Growth of InZnP/ZnS Core/Shell Quantum Dots with Wide-range and Refined Tunable Photoluminescence Wavelength, *Dalton Trans.*, 2020, **49**(18), 6119–6126.

36 J. J. Calvin, *et al.*, Observation of ordered organic capping ligands on semiconducting quantum dots via powder X-ray diffraction, *Nat. Commun.*, 2021, **12**, 2663.

37 **ICDD PDF-2**, *entry 00-032-0452*, 2003.

38 B. J. Skinner, Unit-cell edges of natural and synthetic sphalerites, *Am. Mineral.*, 1961, **46**, 1399–1411.

39 P. C. J. Clark and W. R. Flavell, Surface and Interface Chemistry in Colloidal Quantum Dots for Solar Applications Studied by X-Ray Photoelectron Spectroscopy, *Chem. Rec.*, 2019, **19**(7), 1233–1243.

40 H. Virieux, *et al.*, InP/ZnS Nanocrystals: Coupling NMR and XPS for Fine Surface and Interface Description, *J. Am. Chem. Soc.*, 2012, **134**(48), 19701–19708.

41 M. D. Healy, *et al.*, The reaction of indium(III) chloride with tris(trimethylsilyl)phosphine: a novel route to indium phosphide, *J. Chem. Soc., Chem. Commun.*, 1989, (6), 359–360.

42 R. Franke, *et al.*, Auger parameters and relaxation energies of phosphorus in solid compounds, *J. Electron Spectrosc. Relat. Phenom.*, 1991, **56**(4), 381–388.

43 E. J. Luber, Md H. Mobarok and J. M. Buriak, Solution-Processed Zinc Phosphide (α-Zn3P2) Colloidal Semiconducting Nanocrystals for Thin Film Photovoltaic Applications, *ACS Nano*, 2013, **7**(9), 8136–8146.

44 V. I. Nefedov, *et al.*, A study by XPS and XRS of the participation in chemical bonding of the 3d electrons of copper, zinc and gallium, *J. Electron Spectrosc. Relat. Phenom.*, 1975, **6**(3), 231–238.

45 G. O. Eren, *et al.*, Cadmium-free and efficient type-II InP/ZnO/ZnS quantum dots and their application for LEDs, *ACS Appl. Mater. Interfaces*, 2021, **13**(27), 32022–32030.

46 A. Vikram, *et al.*, Unraveling the Origin of Interfacial Oxidation of InP-Based Quantum Dots: Implications for Bioimaging and Optoelectronics, *ACS Appl. Nano Mater.*, 2020, **3**(12), 12325–12333.

47 D. W. Langer and C. J. Vesely, Electronic Core Levels of Zinc Chalcogenides, *Phys. Rev. B: Solid State*, 1970, **2**(12), 4885–4892, DOI: **10.1103/PhysRevB.2.4885**, American Physical Society, s.l.

48 P. S. Wehner, P. N. Mercer and G. Apai, Interaction of H2 and CO with Rh4(CO)12 supported on ZnO, *J. Catal.*, 1983, **84**(1), 244–247, DOI: **10.1016/0021-9517(83)90103-3**.

49 J. Hao, *et al.*, A facile route to synthesize CdSe/ZnS thick-shell quantum dots with precisely controlled green emission properties: towards QDs based LED applications, *Sci. Rep.*, 2019, **9**, 12048.

50 F. Benkabou, H. Aourag and M. Certier, Atomistic study of zinc-blende CdS, CdSe, ZnS, and ZnSe from molecular dynamics, *Mater. Chem. Phys.*, 2000, **66**(1), 10–16.

51 D. G. Castner, K. Hinds and D. W. Grainger, X-ray Photoelectron Spectroscopy Sulfur 2p Study of Organic Thiol and Disulfide Binding Interactions with Gold Surfaces, *Langmuir*, 1996, **12**(21), 5083–5086.

52 J. A. Peter and C. W. Lee, Electronic and optical properties of CdS/CdZnS nanocrystals, *Chin. Phys. B*, 2012, **21**(8), 087302.

53 X. Gan, *et al.*, TiO2 nanorod arrays functionalized with In2S3 shell layer by a low-cost route for solar energy conversion, *Nanotechnology*, 2011, **22**(30), 305601.

54 V. F. Markov, *et al.*, Structure and composition of chemically deposited In2S3 thin films, *J. Surf. Invest.: X-Ray, Synchrotron Neutron Tech.*, 2014, **8**(4), 659–665.

55 A. Golsheikh, *et al.*, Sonochemical synthesis of reduced graphene oxide uniformly decorated with hierarchical ZnS nanospheres and its enhanced photocatalytic activities, *RSC Adv.*, 2015, **5**, 12726–12735.

56 S. K. Apte, *et al.*, A Facile Template–Free Approach for the Large–Scale Solid–Phase Synthesis of CdS Nanostructures and Their Excellent Photocatalytic Performance, *Small*, 2011, **7**(7), 957–964.

57 G. Hota, S. B. Idage and K. C. Khilar, Characterization of nano-sized CdS-Ag2S core-shell nanoparticles using XPS technique, *Colloids Surf., A*, 2007, **293**(1), 5–12.

58 S. Chen and W. Liu, Preparation and Characterization of Surface-Coated ZnS Nanoparticles, *Langmuir*, 1999, **15**(23), 8100–8104.

59 A. M. Dennis, *et al.*, Suppressed Blinking and Auger Recombination in Near-Infrared type-II InP/CdS Nanocrystal Quantum Dots, *Nano Lett.*, 2012, **12**(11), 5545–5551.

60 K. Wu, *et al.*, Interfacial Charge Separation and Recombination in InP and Quasi-Type II InP/CdS Core/Shell Quantum Dot-Molecular Acceptor Complexes, *J. Phys. Chem. A*, 2013, **117**(32), 7561–7570.

61 Z. Sun, *et al.*, Suppressing the Cation Exchange at the Core/Shell Interface of InP Quantum Dots by a Selenium Shielding Layer Enables Efficient Green Light-Emitting Diodes, *ACS Appl. Mater. Interfaces*, 2022, **14**(13), 15401–15406.